Article

Super Crystal Structures of Octahedral c-InO Nanocrystals

Weigang Lu, Qingsheng Liu, Zhaoyong Sun, Jibao He, Chidi Ezeolu, and Jiye Fang

J. Am. Chem. Soc., **2008**, 130 (22), 6983-6991 • DOI: 10.1021/ja078303h • Publication Date (Web): 08 May 2008

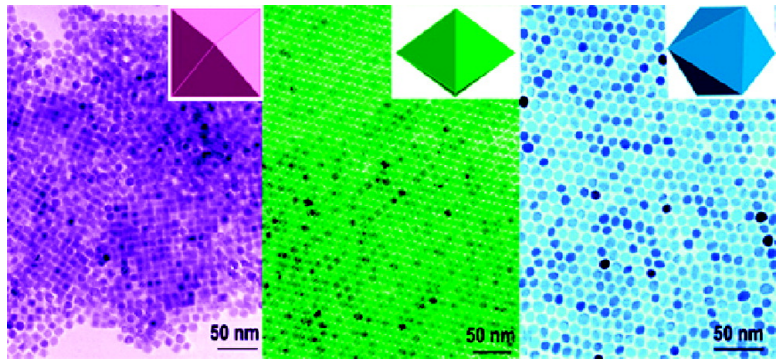

More About This Article

Additional resources and features associated with this article are available within the HTML version:

- Supporting Information
- Links to the 4 articles that cite this article, as of the time of this article download
- Access to high resolution figures
- Links to articles and content related to this article
- Copyright permission to reproduce figures and/or text from this article

View the Full Text HTML

J|A|C|S
ARTICLES

Published on Web 05/08/2008

Super Crystal Structures of Octahedral c-In_2O_3 Nanocrystals

Weigang Lu,[†,⊥] Qingsheng Liu,[†,○] Zhaoyong Sun,[‡] Jibao He,[§] Chidi Ezeolu,[‡] and Jiye Fang*[,‡,||]

Department of Chemistry and AMRI, University of New Orleans, New Orleans, Louisiana 70148, Department of Chemistry, State University of New York at Binghamton, Binghamton, New York 13902, Coordinated Instrumentation Facility, Tulane University, New Orleans, Louisiana 70118, and Multidisciplinary Program in Materials Science and Engineering, State University of New York at Binghamton, Binghamton, New York 13902

Received October 30, 2007; E-mail: jfang@binghamton.edu

Abstract: The three-dimensional self-assembly of a nanocrystal superlattice, i.e., a super crystal, has attracted increasing attention. The small building blocks for assemblies are usually spherical nanocrystals. Recent progress indicates that it is possible to achieve a super crystal using cubic nanocrystals. We further analyze and describe two-dimensional and some three-dimensional assemblies of uniform cubic-phase In_2O_3 nanocrystals with an *octahedral* shape. In this article, we demonstrate our amazing observations on these kinds of super crystals (or superlattices) as a model system, report their scale in at least tens of microns, and show other interesting features such as steps, terraces, kinks, and vacancies which are similar to those from a single crystal. Based on electron microscopy observations, three types of well-defined *octahedral* nanocrystal packed structures in such super crystal systems are also identified. The investigation of octahedral super crystal systems provides an alternate direction in research that may extend the interest of superlattice study to a broad spectrum by enriching and varying the shape of elemental building blocks. This may potentially result in new concepts and more challenging applications such as soft X-ray photonics.

Introduction

The three-dimensional (3D) self-assembly of a nanocrystal (NC) superlattice,[1–4] i.e., a super crystal (SC), has attracted increasing attention in the field of nanoscience and nanotechnology, which could result in novel concepts, new devices, and some emerging high-performance applications. Observation of the periodically packed structures[1–3,5–9] in an SC is crucial to understanding the superlattice growth mechanism and to predicting the collective properties. The building blocks of most 3D SC systems which have been achieved so far, however, are only spherical NCs. There have been very rare reports that release the manipulation and analysis of 3D SCs based on other types of NCs, including cubic,[10] octahedral,[11] and truncated octahedral[12,13] building blocks. Recent success of high-quality NC synthesis enables us to further focus our efforts on the exploration of 3D SCs with nonspherical building blocks. Here we present our amazing observations of 3D SCs consisting of octahedral In_2O_3 NCs, as a model system, with the size of at least tens of microns in scale. For the first time, three types of well-defined octahedral NC packing structures in this SC system were observed and identified. Scanning Electron Microscopy (SEM) analysis reveals that the surface of such SCs is flat, dense, and sufficiently large. It was further determined that terrace surfaces with uniformed steps could be present in these SCs. Our results demonstrate different superlattice structures and close-packing efficiencies from those in which identical spheres are involved and sphere packing theory is applied. Our observation provides preliminary information revealing how those octahedral NCs could be packed into SCs and demonstrates a new starting point of an avenue in manipulating, investigating, and probably utilizing novel SCs built by octahedral NCs.

For identical spheres, both the hexagonal close-packing (hcp) and cubic close-packing (ccp) give the highest packing efficiency, 74.04%. Nevertheless, NCs could be present in various

[†] University of New Orleans.
[‡] Department of Chemistry, State University of New York at Binghamton.
[§] Tulane University.
[||] Multidisciplinary Program in Materials Science and Engineering, State University of New York at Binghamton.
[⊥] Present address: Innovatek, Inc., 350 Hills St., Richland, WA 99354-5511.
[○] Present address: Department of Chemistry, Texas A&M University, College Station, TX 77842-3012.

(1) Shevchenko, E. V.; Talapin, D. V.; Kotov, N. A.; O'Brien, S.; Murray, C. B. *Nature* **2006**, *439*, 55–59.
(2) Redi, F. X.; Cho, K.-S.; Murray, C. B.; O'Brien, S. *Nature* **2003**, *423*, 968–971.
(3) Xia, Y.; Gates, B.; Li, Z.-y. *Adv. Mater.* **2001**, *13*, 409–413.
(4) Zeng, H.; Li, J.; Liu, J. P.; Wang, Z. L.; Sun, S. *Nature* **2002**, *420*, 395–398.
(5) Shevchenko, E. V.; Talapin, D. V.; Murray, C. B.; O'Brien, S. *J. Am. Chem. Soc.* **2006**, *128*, 3620–3637.
(6) Puntes, V. F.; Krishnan, K. M.; Alivisatos, A. P. *Science* **2001**, *291*, 2115–2117.
(7) Desvaux, C.; Amiens, C.; Fejes, P.; Renaud, P.; Respaud, M.; Lecante, P.; Snoeck, E.; Chaudret, B. *Nat. Mater.* **2005**, *4*, 750–753.
(8) Sun, S.; Murray, C. B. *J. Appl. Phys.* **1999**, *85*, 4325–4330.
(9) Peng, X.; Manna, L.; Yang, W.; Wickham, J.; Scher, E.; Kadavanich, A.; Alivisatos, A. P. *Nature* **2000**, *404*, 59–61.
(10) Li, F.; Delo, S. A.; Stein, A. *Angew. Chem., Int. Ed.* **2007**, *46*, 6666–6669.
(11) Song, Q.; Ding, Y.; Wang, Z. L.; Zhang, Z. J. *J. Phys. Chem. B* **2006**, *110*, 25547–25550.
(12) Wang, Z. L. *J. Phys. Chem. B* **2000**, *104*, 1153–1175.
(13) Zheng, R.; Gu, H.; Xu, B.; Fung, K. K.; Zhang, X.; Ringer, S. P. *Adv. Mater.* **2006**, *18*, 2418–2421.

shapes and morphologies, and the preparation of nonspherical NC self-assembly system may add one more dimension to the determination of its superlattice structure and to the exploration of potential new applications. In order to achieve a nonspherical NC SC, one of the key issues is that NCs must be monodispersed not only in size but also in shape while the surface characteristics of the NCs, including van der Waals, steric, or dipolar interactions, must be well-controlled. In_2O_3, a transparent conductor[14,15] that can be widely used for example in computer touch screens, is present in either the cubic phase (c-In_2O_3)[16] or hexagonal phase (h-In_2O_3).[17] Highlighted by our previous success of octahedral In_2O_3 NC synthesis,[16] in this article we report our recent assembly manipulation and amazing observation of 2D and 3D In_2O_3 SCs as a model system, demonstrating an alternate direction of manipulating and studying NC self-assembly. Such SCs without tetrahedral fillings (or with tetrahedral holes) could achieve a packing efficiency as high as 66.67%.

Experimental Section

Synthesis of c-In_2O_3. In a typical experiment, 0.42 mmol of indium acetate (99.99%, Alfa Aesar), 0.60 mL of oleic acid (90%, Aldrich), and 0.55 mL of oleylamine (70%, Aldrich) were mixed with 7.0 mL of hexadecane (99+%, Aldrich) in a three-neck round-bottom flask equipped with a condenser. Standard air-free techniques were used, and the mildly stirred mixture was vacuumed at room temperature for 15 min. After being purged twice with argon gas, the mixture was heated to 110 °C and kept for 70 min within the vacuum. 1.5 mmol of trimethylamine *N*-oxide (TMNO, 98%, Aldrich) was then added into the vigorously stirred mixture under an argon stream when its temperature was reduced to 100 °C. The system was then heated and refluxed for 2 h while a dynamic multiple-injection[18,19] operation was also applied. The resulting turbid mixture was cooled down to room temperature. The c-In_2O_3 NCs, which are a gray precipitate and can be completely dispersed in hexane, were separated from the reaction mixture by adding sufficient amounts of anhydrous ethanol and collected by a subsequent centrifugation. Highly monodisperse c-In_2O_3 NCs suspended in hexane, in which they are octahedral in shape as shown below, could be obtained after a standard size-selection post-treatment[20] using a pair-solvent of anhydrous hexane and ethanol. These NCs are actually coated with a thin organic layer which made them stable in a nonpolar solvent.

Self-Assemblies and EM Sample Preparation. Self-assembly of the highly monodisperse octahedral c-In_2O_3 suspensions in a mixed solvent containing 95 wt% of anhydrous hexane and 5 wt% of anhydrous ethanol was conducted through three pathways, designated hereafter as a "slow process", "medium process", and "fast process", in which the rates of solvent evaporation were different by carefully controlling the total pressure. The transmission electron microscopy (TEM) samples were prepared on 200 mesh copper grids coated with Formvar/carbon (product code: 01801, from Ted Pella Inc.) at room temperature. One drop of In_2O_3 NC suspension was introduced on a copper grid which was hung by a pair of self-closing TEM tweezers. The rate of solvent evaporation could be altered by placing the grid system in various environments, e.g., in a desiccator which was connected to a vacuum pump (fast process), in ambient conditions (medium process), and in a desiccator with saturation vapor of hexane which was from a small beaker of hexane solvent presented (slow process). The number of layers (thickness of a sample) could be adjusted by varying the concentration of the In_2O_3 NC suspension. The SEM samples were prepared on Si wafers in different evaporation conditions at room temperature. A sufficient amount of concentrated In_2O_3 NC suspension was transferred into a vial in which a piece of Si wafer was preplaced on the bottom. The In_2O_3 NCs were then precipitated and assembled while the solvent was evaporated in various rates, designated as a "fast process", "medium process", and "slow process". In the fast process, the vial (without a cap) containing the In_2O_3 NC suspension and the wafer was moved into a desiccator equipped with a NALGENE Repairable Hand Vacuum Pump (VWR, 6131-0010) and a TRACEBLE vacuum meter (VWR) which is illustrated in the Supporting Information[21] (if necessary, a buffer vacuum bottle may be series-connected between the desiccator and the pump). The total inner vacuum was controlled at ~ -15 inHg, and the self-assembly was completed within a period of $\sim 8-12$ h. The same setup was used to conduct the medium process with an average vacuum of ~ 5 inHg, and the assembly could be achieved for ~ 2 days. In the slow process, no vacuum was applied and the vial with a loose-closed cap was placed in an ambient environment until all of the solvent was evaporated "naturally". This process normally required 2 or more weeks, depending on several other variants. All of the SEM specimens were annealed in a tube furnace which was preset at 400 °C for 8 min in air before the observation.

Sample Characterization. TEM and high-resolution TEM (HRTEM) images were collected using JEOL 2010 microscopes operating at 200 kV. SEM images were recorded on Leo 1530VP, Hitachi 3400, and Zeiss Supra 55VP Field Emission Scanning Electron Microscopes.

Results and Discussion

2D Monolayer Assemblies. We used a regular octahedron to interpret the self-assembled structure although a thin layer of organic molecules was coated on the surface of the real NCs. The regular octahedron is the platonic solid P_4 with 6 polyhedron vertices, 12 polyhedron edges, and 8 equivalent equilateral triangular faces.[22] Experimentally, we observed these projection images, indeed. As demonstrated in Figure 1, several self-assembled patterns of c-In_2O_3 NCs, dominated by certain types of projected images, could be achieved by controlling the NC precipitation rate through a variation of total vapor pressure and solvent composition when the self-assembly was carried out, although the areas of these monolayer patterns are very limited and the NCs are a little truncated. To better understand the TEM projection image of an octahedral NC from various types of assembled orientations, the 3D structure and 3D drawing of an octahedron are presented in Supplementary Figure S1 (a and b, respectively, in the Supporting Information), indicating that the surfaces of the octahedral NC are dominated by {111} facets, the side surfaces are {110}, and the side edges are ⟨110⟩. Supplementary Figure S1 (c−e) also shows mathematical models of the three most typical 2D regular octahedral NC projections. In Figure 1a which was recorded from a fast-processed sample (although the chance is seldom), the TEM projection is along the ⟨001⟩ axis direction and most of the NCs sit on one of their octahedral vertices, stabilized on the substrate

(14) Gordon, R. G. *MRS Bull.* **2000**, *25*, 52–57.
(15) Kong, X. Y.; Wang, Z. L. *Solid State Commun.* **2003**, *128*, 1–4.
(16) Liu, Q.; Lu, W.; Ma, A.; Tang, J.; Lin, J.; Fang, J. *J. Am. Chem. Soc.* **2005**, *127*, 5276–5277.
(17) Lee, C. H.; Kim, M.; Kim, T.; Kim, A.; Paek, J.; Lee, J. W.; Choi, S.-Y.; Kim, K.; Park, J.-B.; Lee, K. *J. Am. Chem. Soc.* **2006**, *128*, 9236–9327.
(18) Lu, W.; Gao, P.; Jian, W. B.; Wang, Z. L.; Fang, J. *J. Am. Chem. Soc.* **2004**, *126*, 14816–14821.
(19) Qian, C.; Kim, F.; Ma, L.; Tsui, F.; Yang, P.; Liu, J. *J. Am. Chem. Soc.* **2004**, *126*, 1195–1198.
(20) Lu, W.; Fang, J.; Stokes, K. L.; Lin, J. *J. Am. Chem. Soc.* **2004**, *126*, 11798–11799.
(21) Refer to Supplementary Figure S5.
(22) Weisstein, E. W."Octahedron." from MathWorld -- A wolfram web resource. http://mathworld.wolfram.com/Octahedron.html(1990).

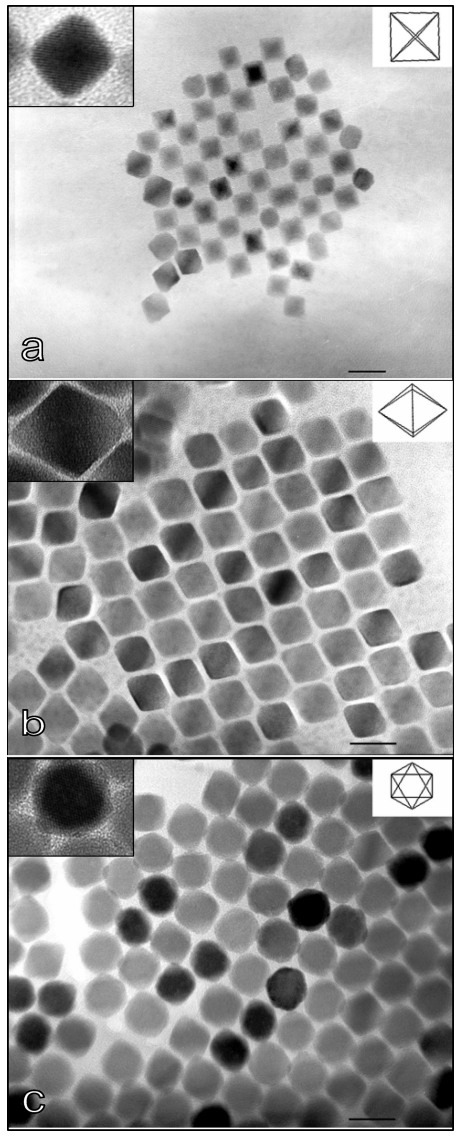

Figure 1. TEM images of monolayer self-assembly patterns consisting of c-In2O3 NCs with different projection axes. Image projection direction: (a) ⟨001⟩, (b) ⟨110⟩, and (c) ⟨111⟩. The scale bars represent 20 nm.

by supporting each other through other little truncated vertices of adjacent NCs. In Figure 1b which was observed from a medium-processed sample, the TEM projection direction is a ⟨110⟩ orientation, and it is believed that the assembled pattern is stabilized by placing slightly truncated {110} facets of the NC on the substrate and by supporting each other through maximum contact of their {111} facets of adjacent NCs.[23] Obviously, this type of assembly is more stable than that in the previous situation (a). It therefore answers why a minor number of NCs sat in such an orientation (projection along ⟨110⟩) can be observed in Figure 1a. Figure 1c gives the most stable model of an assembled pattern, in which the TEM projection axis is along the ⟨111⟩ direction and the NC sits on the substrate with a {111} facet. This type of pattern was, in most times, observed from a slow-processed sample.

2D Multilayer Assemblies. The monolayer c-In_2O_3 NC self-assembly patterns can be extended to multilayer NC superlattices (i.e., 3D structure) on a TEM grid by carefully tuning up the NC concentration in their suspensions. A 3D close-packed structure of octahedral NCs is different from that of traditional colloids, spherical NCs. For identical spheres or monodisperse spherical NCs to pile up a close-packed assembly, a hexagonal pattern in each layer must be formed and the additional layers are often stacked in a sequence of either ABABAB. . . (hcp) or ABCABC. . . order (ccp or fcc), both giving the highest packing efficiency, although it has been reported that fcc might be slightly more energetically favored.[24] In the case of octahedral NCs (e.g., c-In_2O_3), nevertheless, the periodic packing structure and packing efficiency are totally different. Based on the observed TEM images shown in Figures 2–4, three different types of self-assembled patterns of c-In_2O_3 octahedral NCs have been identified.

Type I, [001] projected pattern: each octahedral NC sits on a vertex and two kinds of assembly patterns were observed: (1) NCs are orientated by contacting two other vertices of two adjacent NCs to form a monolayer as shown in Figure 1a. An HRTEM image of an NC in such a pattern is presented in the insert of Figure 1a, as well as in Figure 2c. Since the measured *d*-spacing (2.50 Å) is consistent with that of lattice planes {400}, the NC packing configuration is therefore assigned the same as shown in Model-I2 mentioned below (also refer to Supplementary Figure S2b). No multilayered pattern was observed in this packing configuration. (2) NCs are stabilized by facing the same type of side edges, i.e., by contacting two {110} edges of two adjacent NCs, resulting in a denser packing monolayer (Figure 2a). NCs with the same projection direction in the second layer may sit by their bottom vertices either on the top vertices of NCs in the first layer or on the joint point of four vertices from four adjacent NCs from the first layer and surrounded by these four NCs, depending on their distort-defect in packing (Figure 2b). NCs in the third layer are added by reaching the positions that the NCs in the first layer take and so on for the next layers. In the former case (top-vertex to bottom-vertex), the coordination number of each NC is 8 and the sequence of layers arises as AAAAAA. . . (Figure 2g). The NC packing configuration can be designated as Model-I1 (Supplementary Figure S2a). It can also be calculated that the octahedral NCs should theoretically occupy $^1/_3 = 33.33\%$ of the space in this packing structure, whereas in the latter case, the coordination number of each NC is 12 and the sequence of layers arises as ABABAB. . . (Figure 2i). The NC packing configuration can be designated as Model-I2 (Supplementary Figure S2b). Since only tetrahedral hole spaces are generated among the NCs, it can be calculated that the packing efficiency is $^2/_3 = 66.67\%$. Although it is difficult to directly identify the stacking structure in Figure 2b and to differentiate it between these two models, it is worth mentioning that a considerable number of Moiré patterns could be observed in this TEM image of the multilayer assembly (Figure 2b). Moiré patterns can be formed by interfering two sets of TEM images that have nearly common periodicities, indicating that there are at least 2 layers of NCs in most sites (Figure 2b). Since most of Moiré fringes observed in Figure 2b are in the shape of a "square" rather than a "triangle", we deduce that the two sets of TEM images that originate a square Moiré pattern must be identical and slightly rotated along their projection direction. Obviously, only two NCs stacked in the way of top-vertex to bottom-vertex, i.e., the AAAAAA. . . layer stacking sequence, may exhibit such a phenomenon although this is a higher

(23) The "gap" between two {111} facets of the neighboring NCs is actually filled by the coated organic layer.

(24) Woodcock, L. V. *Nature* **1997**, *385*, 141–143.

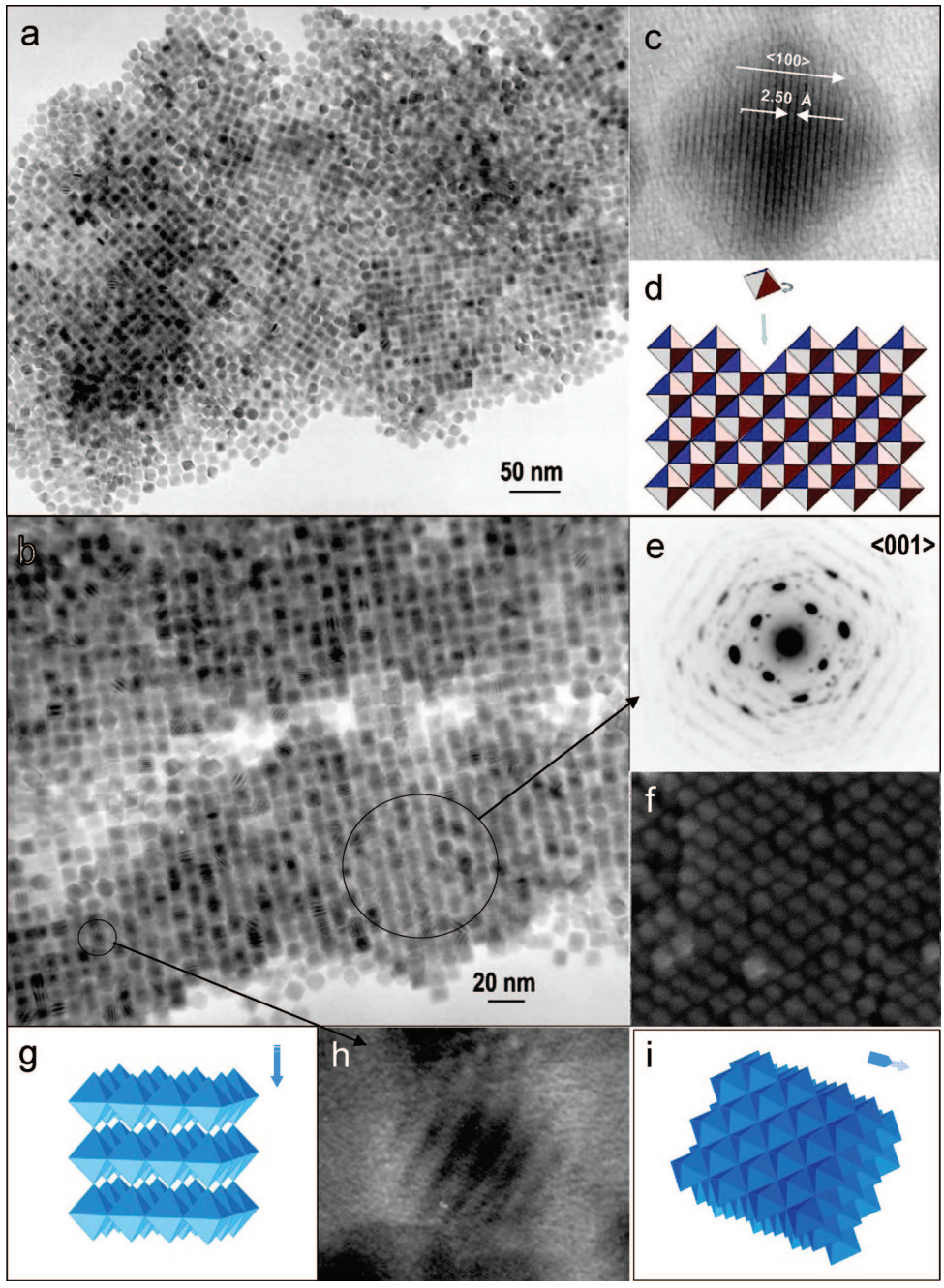

Figure 2. EM images of c-In_2O_3 NC self-assembled patterns with a projection direction of ⟨001⟩ and related crystal structures. The self-assemblies were achieved by controlling the NC precipitation rate through a variation of total vapor pressure and solvent composition. (a) TEM image of monolayer self-assembly pattern; (b) TEM image of double-layer self-assembly pattern; (c) high-resolution TEM (HRTEM) image of an octahedral c-In_2O_3 NC projected in direction of ⟨400⟩ with a measured lattice *d*-spacing of 2.50 Å; (d) a carton showing the structure of monolayer-assembled pattern; (e) a selected area electron diffraction (SAED) pattern, for which more than 40 c-In_2O_3 NCs were included; (f) Field emission SEM image of multilayer self-assembly pattern; (g) structural model showing type I assembly with a packing efficiency of 33.33% (top-down view: ⟨001⟩ projection direction); (h) HRTEM image of "one" NC, showing a Moiré pattern; (i) structural model showing a kind of type I assembly with a packing efficiency of 66.67% (top-down view: ⟨001⟩ projection direction).

surface-energy model compared to the other. If the assembled NC pattern we observed in Figure 2b stacked in the ABA-BAB... layer sequence, Moiré fringes in the shape of a "triangle" would be observed due to the NC−NC connection on their {110} edges. Figure 2e is a selected area electron diffraction (SAED) pattern under a projection direction of ⟨001⟩, for which more than 40 c-In_2O_3 NCs were included. An image (Figure 2f) taken from a field-emission scanning electron microscopy (FE-SEM), as alternate evidence, further supports this deduction.

Type II, [110] projected pattern: Figure 3a demonstrates a double-layer pattern in which Moiré fringes can also be determined as shown in the insert (Figure 3c). In this type of assembly pattern, an octahedral NC sits on a slightly truncated {110} facet (i.e., a {110} "edge") and is supported by contacting two vertices of two adjacent NCs in the first row. In order to further stabilize the pattern, NCs built in the next row have to contact their vertical {110} edges with those of their nearest-neighbor NCs, enclosing polyhedral unoccupied spaces (refer to Figure 3d). There are at least three possible models for

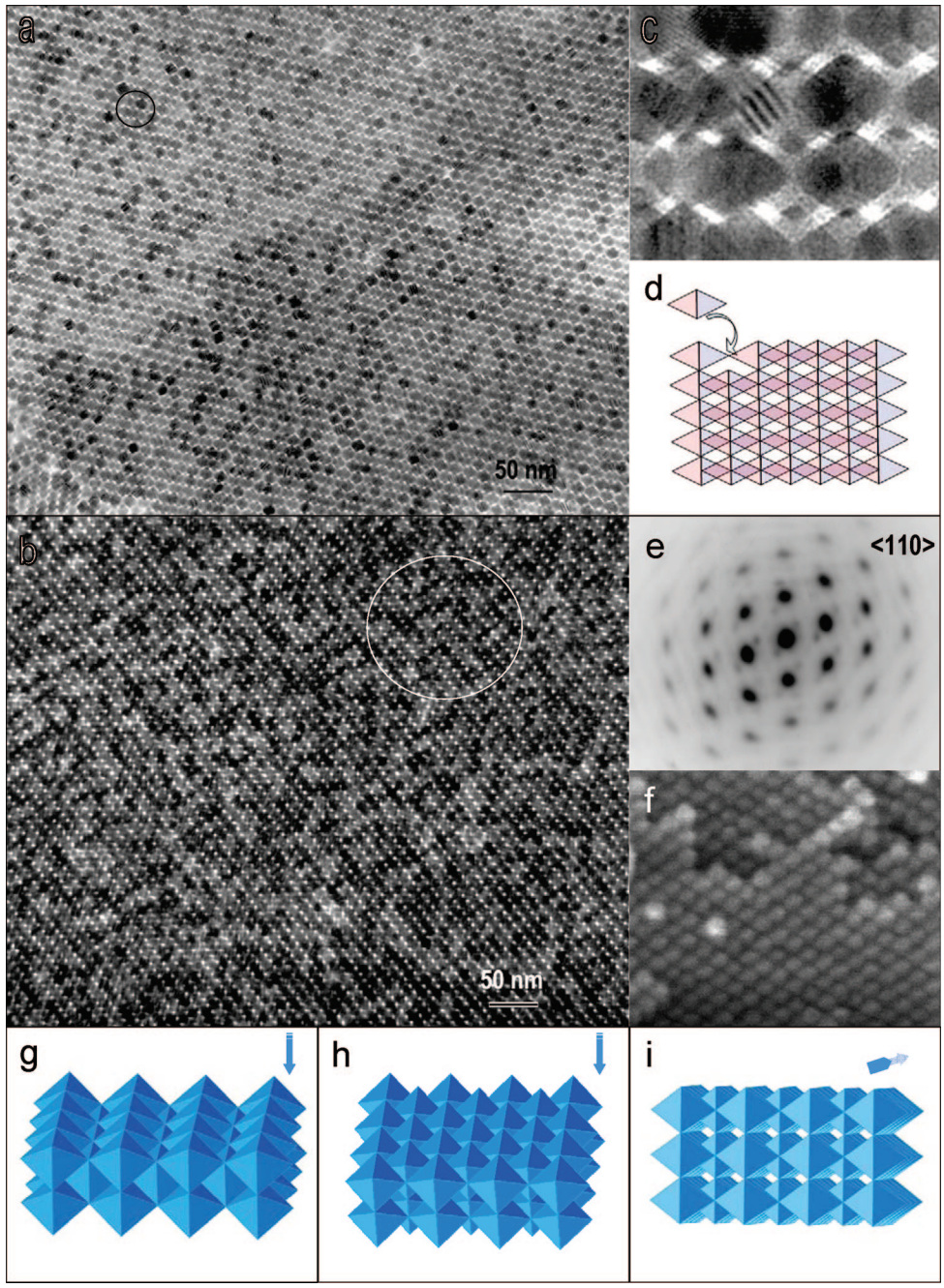

Figure 3. EM images of c-In_2O_3 NC self-assembled patterns with a projection direction of ⟨110⟩ and related crystal structures. The self-assemblies were achieved by controlling the NC precipitation rate through a variation of total vapor pressure and solvent composition. (a) TEM image of double-layer self-assembly pattern; (b) TEM image of multilayer self-assembly pattern; (c) selected high-resolution TEM (HRTEM) image of double-layer self-assembly pattern projected in direction of ⟨110⟩, showing Moiré fringes; (d) a carton showing the structure of monolayer-assembled pattern with a projection direction of ⟨110⟩; (e) selected area electron diffraction (SAED) pattern under projection direction of ⟨110⟩, for which more than 50 c-In_2O_3 NCs were included; (f) Field-emission SEM image of multilayer self-assembly pattern; (g−i): structural models under type II assembly with a packing efficiency of 66.67%; (g) Model-II1, top-down view; (h) Model-II2, top-down view; (i) Model-II3, front-back view (refer to the context).

packing a 3D pattern (multilayer structure). Model-II1: NCs with the orientation the same as the others sit on the hole spaces by their {110} edge and taking positions in a half-NC distance (i.e., half-side-length) higher (or lower) than the layer of the surrounding NCs and contacting the {110} side edges with the nearest-neighbor NCs, generating the second layer and tetrahedral unoccupied spaces (Figure 3g). NCs with the same packing configuration are alternately added on top of {110} facets of NCs in the first and second layers by sitting on their slightly truncated {110} facets, forming the third and fourth layers, and so on. Looking down along the projection direction, stacked NC linear chains along the vertical axis ⟨110⟩ could be observed, and each such NC chain is surrounded by four other similarly assembled NC chains by contacting {111} facets. In this model, the layer-packing sequence is ABABAB. . ., whereas the row-stacking sequence in each layer is AAAAAA. . . (every stacking row in a layer is "separated" by unoccupied spaces). Model-II2: Compared to Model-II1 (Figure 3g), the unoccupied spaces are filled by NCs which make the orientation the same as the others and stay in the same layer of the surrounding NCs by partially contacting the {111} triangular faces to each other in order to minimize the surface energy. NCs with the same

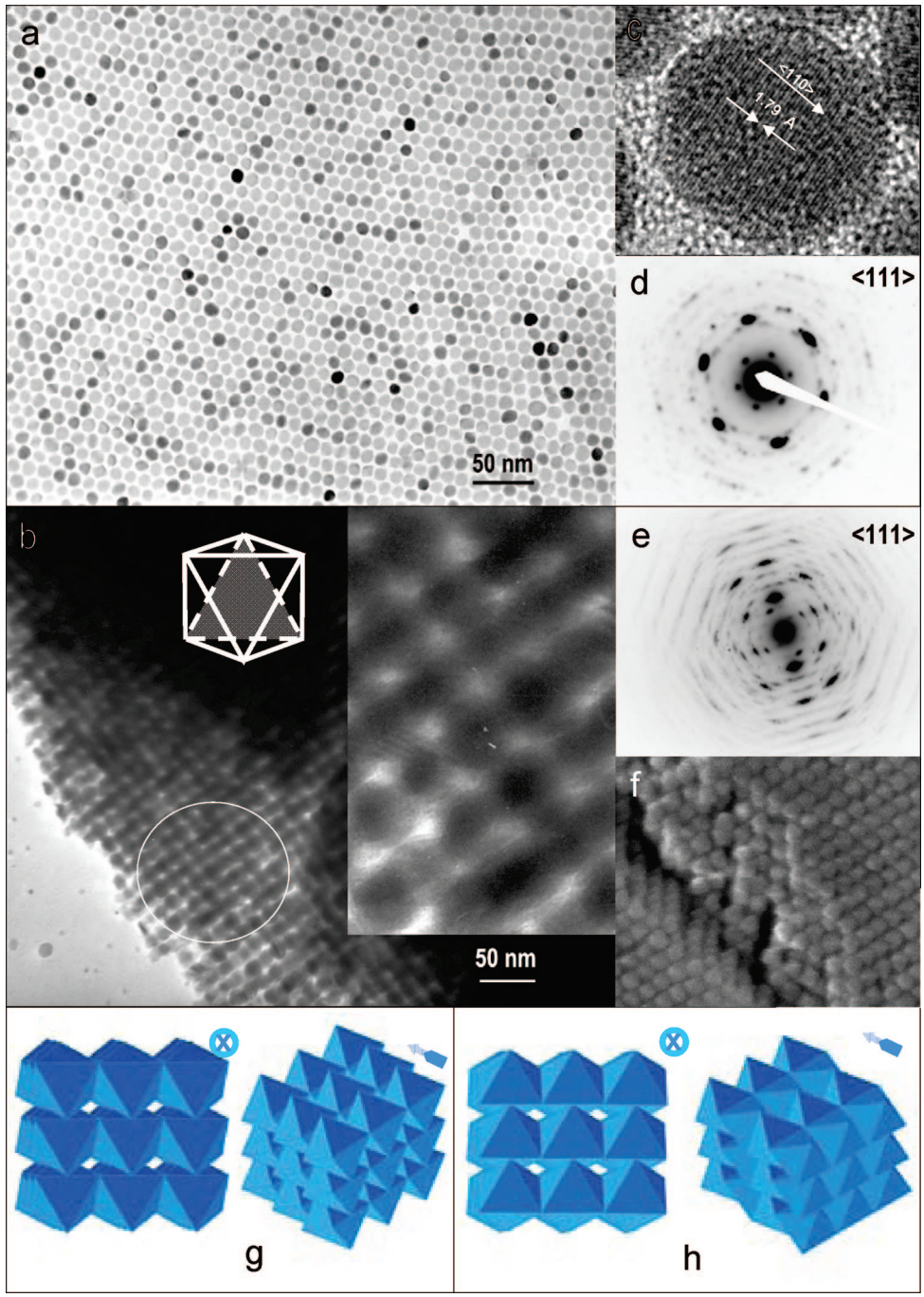

Figure 4. EM images of c-In_2O_3 NC self-assembled patterns with a projection direction of ⟨111⟩ and related crystal structures. The self-assemblies were achieved by controlling the NC precipitation rate through a variation of total vapor pressure and solvent composition. (a) TEM image of monolayer self-assembly pattern; (b) TEM image of multilayer self-assembly pattern (insert is a high-magnification image); (c) high-resolution TEM (HRTEM) image of an NC projected in direction of ⟨111⟩ with a measured lattice *d*-spacing of 1.79 Å in ⟨440⟩; (d) selected area electron diffraction (SAED) of monolayer self-assembled pattern projected in direction of ⟨111⟩; (e) selected area electron diffraction (SAED) of multilayer self-assembled pattern projected in direction of ⟨111⟩; (f) Field-emission SEM image of multilayer self-assembly pattern, showing a {111} facet; (g) structural Model-III1 under type III assembly with a packing efficiency of 66.67% (front-back view); (h) structural Model-III2 under type III assembly with a packing efficiency of 66.67% (front-back view).

packing configuration are repeatedly added on top {110} facets of NCs in the lower layer by sitting on their slightly truncated {110} facets, forming multiple layers (Figure 3h). Looking down along the projection direction, stacked NC linear chains along the vertical axis ⟨110⟩ could be observed, and each such NC chain is surrounded by four other similarly assembled NC chains by contacting {111} facets. In the second model (Figure 3h), the layer-packing sequence is AAAAAA. . .; however, in each layer the row stacking sequence is ABABAB. . . (every alternate stacking row in a layer has to "shift" a half-NC distance along the direction of the row axis, to avoid actual vertex−vertex contact, to increase the contact area and to enhance the packing efficiency).[18] Model-II3: The structure of the third model is actually the same as that of the second model. The only difference between the two models is that the projection orientation is rotated by 90° (refer to Figure 3i). By tuning the "pattern" of Model-II2 90°, one can see "chains of holes" along

the new projection direction. Each unoccupied "chain" is surrounded by four alternately assembled NC chains.

In all three discussed models, it can be calculated that the octahedral NCs occupy $^2/_3 = 66.67\%$ of the space in the packed structure. Since the {111} planes of NCs are partially shared and result in a decrease of surface energy in the second and third models, we therefore believe that the structure which is expressed by the latter two models (actually, the same structure with different projection directions) is a favorable configuration. Indeed, we have successfully observed patterns of c-In_2O_3 octahedral NCs which possess the structure of Model-II3. Figure 3b demonstrates a multilayer pattern of NCs, indicating a structure the same as Model-II3, which is consistent with the observed SEM image (Figure 3f). The SAED pattern (Figure 3e), in which a group of >100 NCs was selected, taken from the multilayer NC assembly confirms that Model-II3 is a dominant structure. According to Model-II1 (Figure 3g) and Model-II2 (Figure 3h), the coordination number of each NC should be 10, whereas the coordination number in Model-II3 (Figure 3i) is counted as 6 (4 nearest-neighbor NCs in the same plane, one on top and one on bottom).

Type III, [111] projected pattern: For comparison, Figure 4a demonstrates a TEM image of an octahedral NC monolayer close-packed pattern, showing that a short-range, hexagonal order of NCs can be self-assembled in an area as large as a few square micrometers.[16] It can be further observed that all of the octahedral NCs sit on the substrate by their {111} facets and the projection direction is [111] (Figure 4c). Figure 4d shows an SAED pattern measured from a corresponding monolayer assembly (Figure 4a). It should be pointed out that hexagonal ordered assembly is not the only packing configuration that we observed on a monolayer along a [111] projection direction. In fact, monolayer patterns with different NC packing configurations could be achieved, depending on a number of manipulation conditions such as the NC concentration, initial polarity of mixed solvents, and velocity of NC precipitation. As a further example, the packing configuration of assembled NCs in a multilayer pattern is different from that revealed in Figure 4a. As shown in Figure 4b (the circumstance of multilayer superlattices), the first-layer NCs in the first row are close-packed by sharing a plane (001) and contacting adjacent side edges {110} of neighboring NCs. Structurally, there are at least two possible row-stacking sequences in a layer: (1) Every other row is "shifted" by a half-NC distance; i.e., the alternate rows (including the second, fourth, sixth. . . rows) "shift" a half-side-length of an NC in the direction of the row-axis. As a result of such an ABABAB. . . row-staking sequence, the octahedral NCs are packed by contacting their "{110} side edges" and generate isolated tetrahedral empty spaces (Supplementary Figure S3a). (2) Each row of NCs is in the same packing configuration (or in the same relative position) in the direction of the row axis and exhibits an AAAAAA. . . row-stacking sequence. Such a pattern is established through a partial contact between adjacent {111} triangular faces of the two nearest-neighbor NCs from different rows, generating "connected" tetrahedral empty spaces (Supplementary Figure S3b). Obviously, the AAAAAA. . . row-stacking structure should have a minimum NC surface energy compared with the ABABAB. . . configuration. As illustrated in Figure 4g and h, in a structure which contains AAAAAA. . . row-stacking configurations, the coordination number of each NC is 6 (4 nearest-neighbor NCs in the same plane, one on top and one on bottom). This conclusion is also consistent with the TEM image observed as discussed below: we did record a [111] projected superlattice 3D pattern containing an AAAAAA. . . row-stacking structure which shows "holes" in the projection direction, but no ABABAB. . . row-stacking structure which has no "holes" could be determined. Figure 4e is an SAED pattern under a projection direction of ⟨111⟩, for which more than 60 c-In_2O_3 NCs were included.

In order to build up a 3D pattern, there are at least two models for NCs to add the second layer on the first-layer pattern consisting of an AAAAAA. . . row-stacking sequence (it is also the same circumstance for an ABABAB. . . system although we are not discussing it here). For Model-III1, each octahedral NC is "piled up" on one in a lower layer by contacting (111) and (11$\bar{1}$), two adjacent triangular facets, in which the top-facet of an octahedral NC in a lower layer partially facets with the bottom-facet of an octahedral NC in a higher layer (Figure 4g). For Model-III2, each octahedral NC reaches one in a lower layer by contacting (111) and (111) planes, the two adjacent triangular facets, in which the top facet of an octahedral NC in a lower layer maximally facets with the bottom facet of an octahedral NC in a higher layer that has been "twisted" 180° around their vertical projection axis, ⟨111⟩; the NC in the next layer is added by "maximally" contacting (11$\bar{1}$) and (11$\bar{1}$) planes, the two adjacent triangular facets, and so on (Figure 4h). In the former way ((111)−(11$\bar{1}$) packing), the layer-packing sequence is ABABAB. . ., whereas, in the latter way ((111)−(111) packing or (11$\bar{1}$)−(11$\bar{1}$) packing), it is AAAAAA. . . Both structures eventually form chains of (fully or partially) facet-sharing c-In_2O_3 octahedral NCs and surrounded hole spaces viewed along the TEM projection direction. It can be further calculated that in the case of such a close-packed structure the octahedral NCs occupy $^2/_3 = 66.67\%$ of the volume as well.[25] An image (Figure 4f), taken using FE-SEM, further shows a large pattern of such a 3D [111] multilayer assembly.

Feature of 3D Super Crystal. The colloidal c-In_2O_3 octahedral NCs can further grow into a 3D SC, i.e., an artificial crystal or superlattice,[26,27] from the colloidal suspension if the solvent evaporation rate is well controlled so that NCs have sufficient time to find equilibrium superlattice sites on the growing structure.[28] As stated before, we have maintained three rates of solvent evaporation and achieved 3D SCs in different major packing structures, namely type I, II, and III. Although we have not found a one-by-one relationship between the packed structure of an SC and its assembly rate, we realize that there is a very high chance that the type I, II, and III structures are detected from SCs formed through a fast process, medium process, and slow process, respectively, based on our FE-SEM observation to date. This may be attributed to the different dynamic energies during the different associated processes. Low-magnification FE-SEM analysis reveals that the surface of the SC is flat, dense, and sufficiently large at least on a tens of microns scale (Figure 5a). As an example, Figure 5b demonstrates a type-I packed structure on the surface of an SC which was prepared through a fast-processing pathway. Its high-resolution FE-SEM image was shown in Figure 2f. We have

(25) In addition, a [111] projected superlattice 3D octahedral NC pattern possessing ABABAB-row-packing sequence and (111)−(111) layer-packing structure, if it exists, should trap empty spaces in trigonal bipyramidals, which are combined tetrahedral holes.

(26) Bentzon, M. D.; Wonterghem, J. v.; Morup, S.; Thoelen, A.; Koch, C. J. W. *Philos. Mag. B* **1989**, *60*, 169–178.
(27) Shiraishi, K.; Tamura, H.; Takayanagi, H. *Appl. Phys. Lett.* **2001**, *78*, 3702–3704.
(28) Murray, C. B.; Kagan, C. R.; Bawendi, M. G. *Annu. Rev. Mater. Sci.* **2000**, *30*, 545–610.

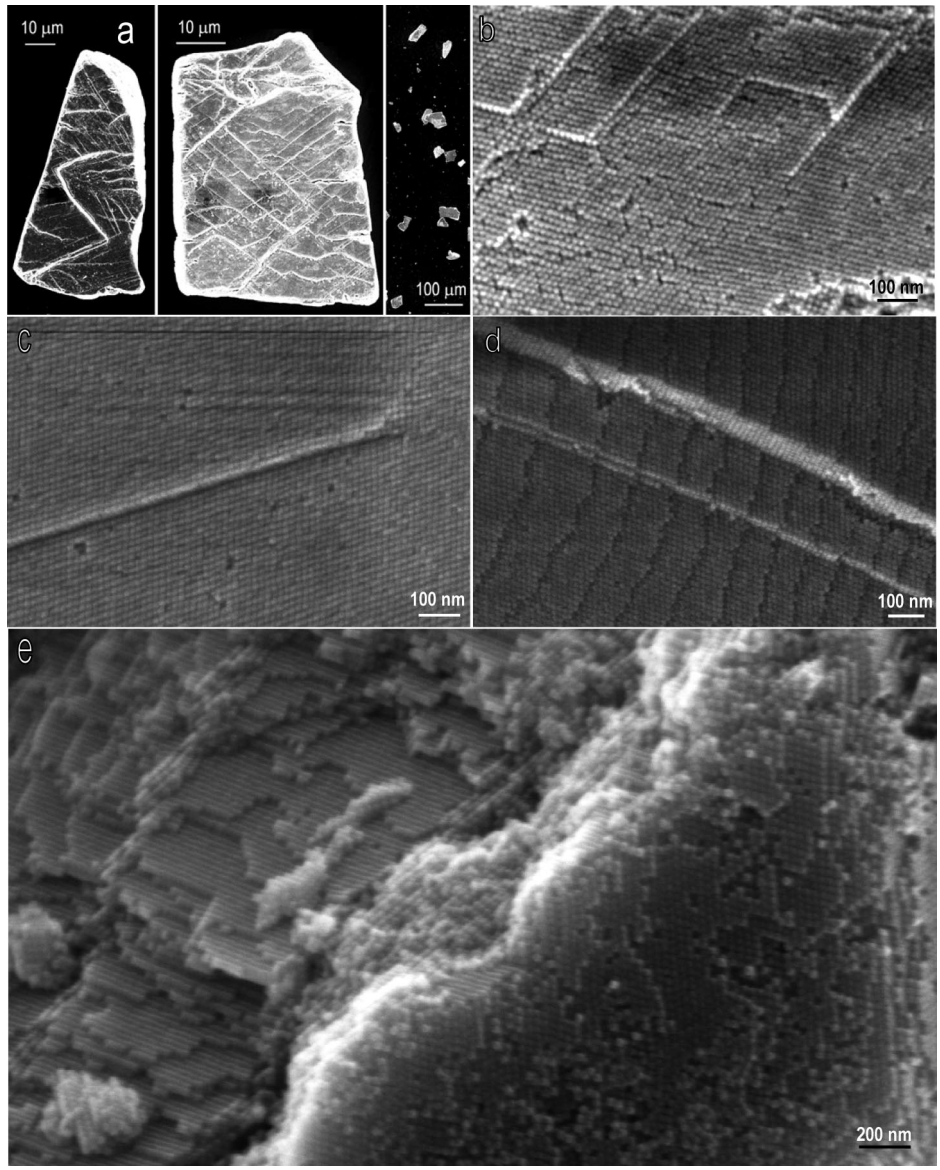

Figure 5. (a) Low-magnification SEM images showing the c-In_2O_3 super crystals, indicating that they are sufficiently large at least on a tens of microns scale. The specimens were stripped from an assembly substrate (Si) and annealed at 400 °C for 8 min; (b) FE-SEM image taken from a fast-processed sample, showing a type-I packed structure at the observed area; (c) FE-SEM image taken from a medium-processed sample, showing a type-II packed structure at the observed area; (d) FE-SEM image taken from a slow-processed sample, showing a type-III packed structure at the observed area; (e) FE-SEM images revealing a piece of type-II packed super crystals. The angle of the sample was tilted to a position where two neighboring surfaces of the superlattice could be seen.

also explored SCs assembled from a medium process, and most FE-SEM images indicate a type-II packed structure as presented in Figure 5c and Figure 3f (high-resolution). We have further tilted the SC sample and observed its neighboring surfaces as shown in Figure 5e. FE-SEM images (Figures 5d and 4f) taken from a slow-processed SC sample exhibit a type-III packed structure at our observed areas. In this type of structure, terrace structures with uniform steps could be observed when a flat surface of an SC was zoomed-in although features like cracks and grooves coexisted as well (Figure 6a). A higher resolution on this surface (Figure 6b) reveals that all the features observed in the 3D superlattice, including steps, terraces, kinks, and vacancies, are the same as those from a single crystal. It can be further identified that the terraces are parallel to the {111} facets. Their length along the profile line in Figure 6b is ~10 NC size, whereas the step height is 1 NC size. For the terrace surface, therefore, the miscut angle from (111) planes is ~3.05° (approximately derived from tan $\theta = {}^1/_{10}$).

Although growth of SCs from various colloidal systems has been extensively studied, it is worth emphasizing the formation of stepped surface structures observed in our octahedral c-In_2O_3 SCs. For a single crystal, a vicinal surface can be made by miscutting at a small angle in a symmetrical direction and reconstructing it in a common way to create a surface characterized by wide terraces separated by monatomic steps.[29] Accounting for the surface area in a colloidal suspension system, capillary force may play an important role in shape changes during the drying process. For example, the suspended NCs in a diluted solution have a tendency to move to the edge and to

(29) Bhattacharjee, S. M.; Mukherji, S. *Phys. Rev. Lett.* **1999**, *83*, 2374–2377.

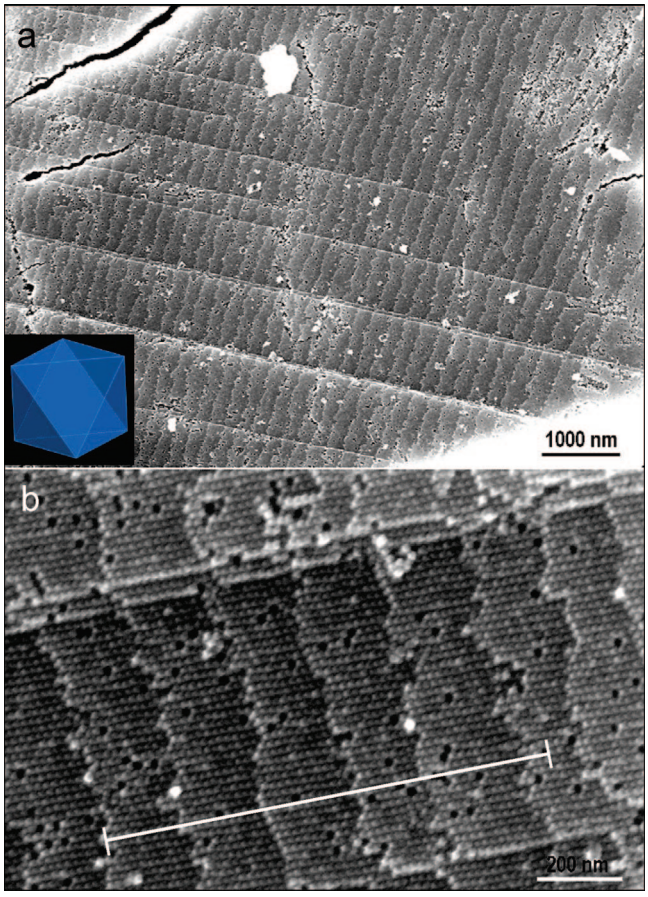

Figure 6. FE-SEM images of a super crystal of c-In_2O_3 NCs. (a) low-magnification image showing a flat and terrace surface structure; (b) zoomed-in image revealing that all the features observed in this 3D super crystal including steps, terraces, kinks, and vacancies are as same as those from a single crystal; the inset in (a) indicates the octahedral NC configuration, corresponding to a packed structural model of type III.

form a ring-like deposit along the perimeter after it dries.[30] Whitesides' group used different shaped PDMS molds and demonstrated a series of two-dimensional structures from millimeter to submillimeter scales based on lateral capillary forces.[31] In a colloidal suspension system, as soon as drying begins, a "foot" forms near the contact line and the height of the drop decreases as well[32] (Supplementary Figure S4). The NCs will be transferred to the "foot" area by the solvent convective flow and accumulate until a gelation occurs near the boundary between the foot and the central part of the drop.[33] If the colloidal concentration is low, most of the NCs will be deposited on the edge of the drop, forming a dense, ring-like pattern along the perimeter.[30] If the concentration of the colloidal system is high, a new foot area will subsequently be solidified on the substrate of colloidal crystals immediately after the foot area is established. By repeating this procedure in our slow-processing evaporation (illustrated in Supplementary Figure S5), a stepped surface structure, i.e., a terrace surface, might be generated. In addition, with a large area covered by the suspension of colloidal NCs, the assembled SC (3D superlattice) may possess a vicinal surface. On the other hand, if the period of precipitation time is sufficiently long, precipitated octahedral NCs will choose the most stable sites/orientation to "settle down" into in order to minimize their surface energy. In this case, the structure in the type-III packing configuration is most likely observed. If the solvent evaporation rate could be steadily increased by varying the total pressure, SCs consisting of octahedral NCs with other types of packing configurations may be generated. Supplementary Figure S6 shows an example in which the image was taken from an SC being prepared through a relatively fast solvent-evaporation pathway (which was much faster than our "fast process" stated above).

Conclusions

In conclusion, we have processed 3D SCs of assembled octahedral c-In_2O_3 NCs as "artificial solids" using a controlled solvent-evaporation approach. We also amazingly observed and identified three types of packing structures. This observation may provide preliminary, but significant information in the direction of NC manipulation and high-performance applications at the level of superlattice or SC with nonspherical NCs. Close-packing of octahedral NCs could result in more complex superlattice structures compared to the assembly of identical spheres as well, demonstrating a new avenue of investigating and utilizing nanostructured materials. This could ultimately enable the generation of other types of superlattices and a fine-tuning of the SC structure and properties. In addition to the assembly of binary SCs, this study provides an alternative research direction, which could broaden the extent of interest of superlattice studies by enriching and varying the shape of elemental NCs, potentially resulting in new concepts and more challenging applications, such as soft X-ray and nanophotonics.

Acknowledgment. This work was supported by the NSF CAREER program (DMR-0731382) and State University of New York at Binghamton. We also thank Dr. Qingfeng Xing for his valuable discussions.

Supporting Information Available: 3D structures of an octahedron, presentations of octahedral orientation of In_2O_3 NC in Models I1 and I2, two row-stacking ways in a layer In_2O_3 NC in Models III1 and III2, schematic illustration of an evaporation process to achieve a 3D super crystal, general schematic illustration and picture of experimental setup to achieve a 3D self-assembled In_2O_3 super crystal pattern, SEM image of a 3D super crystal resulted from an "ultra-fast" solvent-evaporation process. This material is available free of charge via the Internet at http://pubs.acs.org.

JA078303H

(30) Deegan, R. D.; Bakajin, O.; Dupont, T. F.; Huber, G.; Nagel, S. R.; Witten, T. A. *Nature* **1997**, *389*, 827–829.
(31) Bowden, N.; Terfort, A.; Carbeck, J.; Whitesides, G. M. *Science* **1997**, *276*, 233–235.
(32) Parisse, F.; Allain, C. *J. Phys. II France* **1996**, *6*, 1111–1119.
(33) Nagayama, K. *Colloid Surf., A* **1996**, *109*, 363–374.